

Amyloid Formation from an α -Helix Peptide Bundle Is Seeded by 3_{10} -Helix Aggregates

Yogendra Singh,^[a] Philip C. Sharpe,^[a] Huy N. Hoang,^[a] Andrew J. Lucke,^[a]
Alasdair W. McDowall,^[b] Stephen P. Bottomley,^[c] and David P. Fairlie*^[a]

Abstract: Transformation of proteins and peptides to fibrillar aggregates rich in β sheets underlies many diseases, but mechanistic details of these structural transitions are poorly understood. To simulate aggregation, four equivalents of a water-soluble, α -helical (65%) amphipathic peptide (AEQLL-QEAEQLLQEL) were assembled in parallel on an oxazole-containing macrocyclic scaffold. The resulting 4α -helix bundle is monomeric and even more α helical (85%), but it is also unstable at pH 4 and undergoes concentration-dependent conversion to β -sheet aggregates

and amyloid fibrils. Fibrils twist and grow with time, remaining flexible like rope ($>1\ \mu\text{m}$ long, 5–50 nm wide) with multiple strings (2 nm), before ageing to matted fibers. At pH 7 the fibrils revert back to soluble monomeric 4α -helix bundles. During $\alpha\rightarrow\beta$ folding we were able to detect soluble 3_{10} helices in solution by using 2D-NMR, CD and FTIR spectroscopy. This inter-

mediate satisfies the need for peptide elongation, from the compressed α helix to the fully extended β strand/sheet, and is driven here by 3_{10} -helix aggregation triggered in this case by template-promoted helical bundling and by hydrogen-bonding glutamic acid side chains. A mechanism involving $\alpha\rightleftharpoons\alpha_4\rightleftharpoons(3_{10})_4\rightleftharpoons(3_{10})_n\rightleftharpoons(\beta)_n\rightleftharpoons m(\beta)_n$ equilibria is plausible for this peptide and also for peptides lacking hydrogen-bonding side chains, with unfavourable equilibria slowing the $\alpha\rightarrow\beta$ conversion.

Keywords: aggregation • amyloid • beta sheets • helical structures • peptides

Introduction

Over 30 diseases are now thought to be caused by “misfolding” of proteins (e.g., β -amyloid, prions, superoxide dismutase (SOD), amylin, islet amyloid peptide, α -synuclein, Huntingtin, calcitonin, transthyretin, lysozyme, cystatin C, apoli-

poproteins), which undergo structural transitions to β sheets that aggregate into water-insoluble, non-crystalline polymers, called amyloids.^[1] Reasons for misfolding in vivo remain unclear, and the aggregating and precipitating properties of such polypeptides have made it difficult to investigate mechanisms of amyloid formation in vitro. Amyloid structures are long lived and unusually resistant to dissociation and enzymatic degradation. Non-pathological amyloids are now known to occur throughout the human body and in other species^[1a,b,e,2] and it has recently become clearer that living organisms may make use of amyloid for storage or to perform specific biological functions.^[1a,e,f,2] Thus, amyloid formation is not only associated with disease, amyloids may play roles in normal physiology and might conceivably even form from any protein under appropriate conditions (pH, temperature, mutation, chaperones, isomerases, lipid–water transitions).

Although substantial progress has been made towards understanding the preferred sequences, structures and properties of amyloid peptides and proteins,^[1–3] there is still a lack of detailed molecular understanding of intra- and intermolecular interactions that promote early stages of amyloidogenesis. However, amyloid formation across diverse systems

[a] Dr. Y. Singh, Dr. P. C. Sharpe, Dr. H. N. Hoang, Dr. A. J. Lucke, Prof. D. P. Fairlie
Division of Chemistry and Structural Biology
Institute for Molecular Bioscience
The University of Queensland
Brisbane, Qld 4072 (Australia)
Fax: (+61) 733462990
E-mail: d.fairlie@imb.uq.edu.au

[b] Dr. A. W. McDowall
Howard Hughes Medical Institute
California Institute of Technology
Pasadena, CA 91125 (USA)

[c] Prof. S. P. Bottomley
Department of Biochemistry and Molecular Biology
Monash University, Victoria, Clayton, 3800 (Australia)

Supporting information for this article is available on the WWW under <http://dx.doi.org/10.1002/chem.201002500>.

does appear to follow a characteristic kinetic profile, consisting of a number of steps including a lag phase during which nucleation occurs, followed by rapid chain elongation and cooperative association.^[1a,b]

Among many folded structures, α helices have frequently been found to convert to aggregated β sheets but the mechanisms by which they unfold or partially unfold and aggregate are unknown.^[1a] Helical proteins, peptidomimetics and model systems have been used to probe α -helix to β -sheet transformations, including examples of native and mutated proteins, coil-coil and zipper peptides.^[1,4]

An interesting question is whether it is important for α helices to aggregate before they convert to β sheets. Regardless of the starting conformation of the precursor, most amyloid fibers are thought to share a common cross β -structure^[3a,b] assembled from β strands that are arranged into sheets, with strands perpendicular to the fiber length and backbone hydrogen bonds parallel. Structural studies on β -amyloid (A β) and prion fibrils in particular have found in-register parallel strand arrangements (sheets) that may be a feature of peptide assembly in amyloids.^[3a-g]

To test whether aggregates of parallel helices might promote helix-sheet transformations leading to amyloid, we have investigated parallel arrays of a water-soluble, amphipathic, α -helical peptide H-[AEQLQAEQLQEL]-NH₂ (**1**) that is not known^[3h,i,4k] to aggregate or form fibrils. This peptide was also chosen because it contains multiple Gln/Glu residues expected to enhance the water solubility and thought to be important in amyloidosis.^[3a] For example, amyloid formation is enhanced for β -amyloid (A β), β 2-microglobulin, α -synuclein, lysosyme, apolipoproteins, prothymosin and other proteins in acidic media,^[4f,5] where Glu/Asp side chains are protonated to form uncharged hydrogen-bond donors. Mutation to a hydrogen-bonding glutamine side chain in A β (E22Q),^[4f] cystatin C (L68Q)^[5c] and transthyretin (L55Q)^[5d] has been found to promote amyloidosis in vitro/vivo, glutamine-containing yeast prions aggregate to fibrils, Huntingtin protein has a polyglutamine sequence, and polyglutamine proteins are recruited into fibrils.^[6] Thus, polar amide/acid side chains may assist peptide aggregation in vivo.

Synthetic peptides have previously been assembled on templates that can increase the α -helical content in the backbone of the peptide as a result of inter-peptide interactions.^[7] By arraying four copies of peptide **1** in parallel regis-

ter on a template **2**,^[7c,8] which can encourage inter-peptide interactions in **3** (Figure 1), to effectively simulate an aggregated state of four copies of peptide, we considered that a

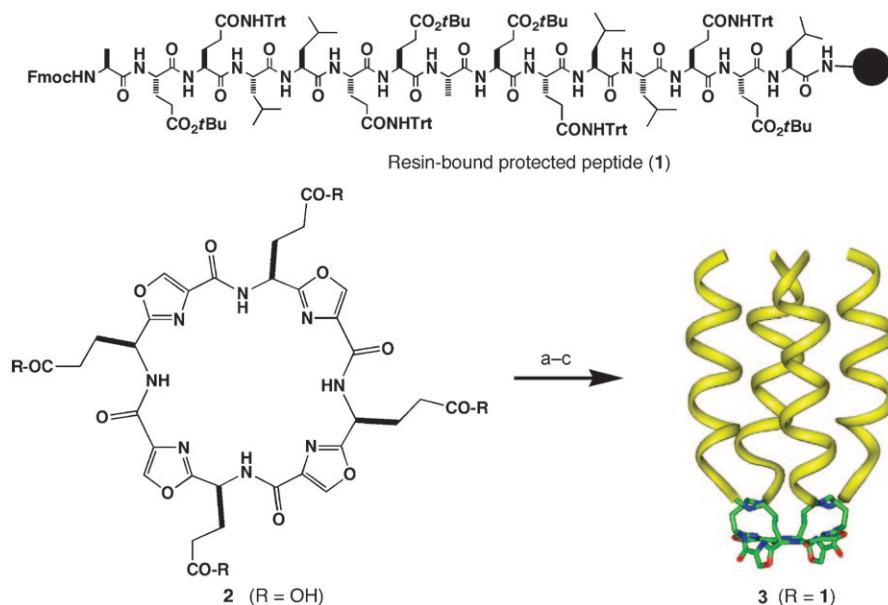


Figure 1. Parallel assembly of four equivalents of peptide **1**. Reagents: a) piperidine/DMF (1:1); b) resin-bound, protected **1**, [benzotriazole-1-yl]-oxytris(dimethyl-amino)phosphonium] hexafluoro-phosphate (BOP), diisopropylethylamine (DIPEA), DMF, RT; c) trifluoroacetic acid (TFA)/1,1,3,3-tetraisopropyl-1,3-disiloxan-1,3-diyl (TIPS)/H₂O (95:2.5:2.5), RT. See the Supporting Information for this figure in colour.

helix-to-sheet transition might be inducible and that intermediates in this case may be soluble enough in water to be identified in solution. Conformational changes in peptides have been achieved previously through, for example, chemical bond O→N-acyl migrations inducing random-coil to β -sheet transformations.^[9] α -Helical coiled-coil peptides have also been shown to form fibrils through interactions of hydrophobic and charged residues.^[4j,10] We now report detection of pH- and concentration-dependent conformational changes that characterise transformation of a monomeric α -helical 4-peptide bundle **3**, via a novel aggregated 3₁₀-helix bundle, to nanofiber aggregates typical of amyloid peptides. Interestingly, in the present case, altering the pH to 7 completely reverses the process at any stage of the transformation to regenerate **3**.

Results and Discussion

Four copies of peptide **1** were assembled on a macrocyclic oxazole-containing template **2** to produce the 4-helix bundle **3** (Figure 1). A novel feature of this synthesis was the addition of multiple equivalents of the resin-bound peptide directly to a solution of macrocycle **2**, a one-pot synthesis that led to high yields of pure 4-helix bundle **3**. The synthesis, purification and characterisation of peptide **1**, template **2** and the template-mounted 4-helix bundle **3** shown in Figure 1

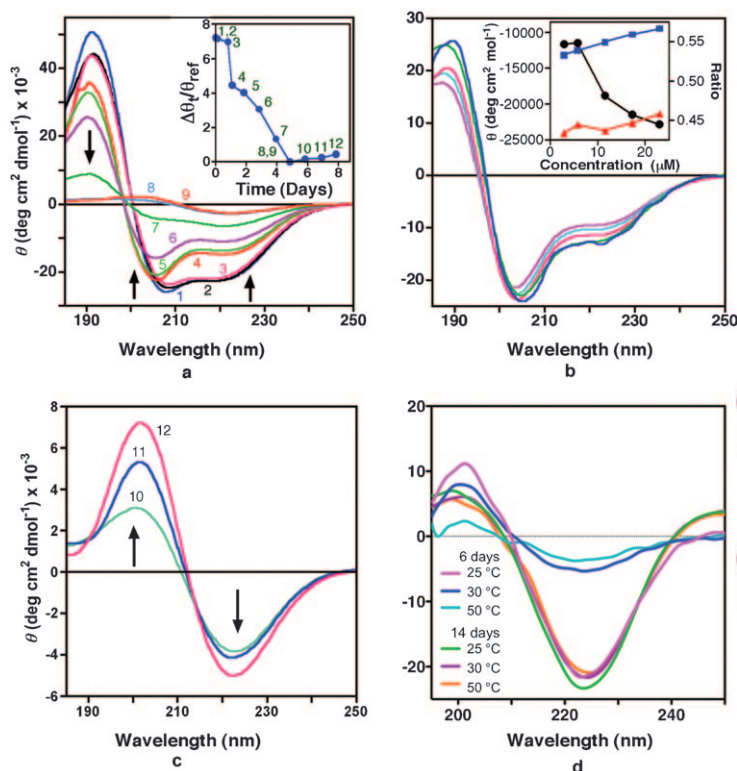


Figure 3. CD spectra for **3**, measured over 0–14 days showing formation of a 3_{10} helix after 24 h and a β sheet after 10 days. a) CD spectrum of compound **3** (59 μM in 50 mm phosphate buffer, 25% MeCN, 25 $^{\circ}\text{C}$, pH 4): zero time (curve 1), 1 h (curve 2), 6 h (curve 3), 1 d (curve 4), 2 d (curve 5), 2.5 d (curve 6), 4 d (curve 7) and 5 d (curve 8; curve 9); curves 4, 5 and 6 are consistent with a 3_{10} helix. Inset: $(\theta_t - \theta_{\text{ref}})/\theta_{\text{ref}}$ (θ_t = molar ellipticity at time t , θ_{ref} = minimum molar ellipticity at 222 nm) versus time over 8 d. For spectra after 6 d see c). b) CD spectra for **3** (2, 6, 12, 17, 23 μM) after ≈ 24 h at pH 4, showing a concentration-dependent reduction of the molar ellipticity that indicates aggregation. Inset: Molar ellipticity versus concentration, showing changes of θ_{222} (blue), θ_{208} (red) and of the ratio $\theta_{222}/\theta_{208}$ (black) after lag phase. c) Investigation of the same solution of **3** as used in a) but aged for 6 (curve 10), 7 (curve 11) and 8 d (curve 12). Molar ellipticity at $\lambda=223$ and 200 nm are consistent with the formation of β sheets. d) Far-UV CD spectra (25–50 $^{\circ}\text{C}$) for isolated fibrils after 6 versus 14 d, showing increased thermal stability upon ageing.

aqueous solutions. Furthermore, there were no corresponding CD spectral changes during the same time that α -helix to β -strand transitions occurred in the presence of phosphoric acid.

The α - to 3_{10} -helix interconversion for peptide bundle **3:** A conformational change in the peptide backbone was observed after several hours at pH 4. For example, CD spectra for **3** at pH 4 had noticeably changed after 26 h (Figure 3 a, curve 4), with a ratio $\theta_{222}/\theta_{205} \approx 0.47$ more typical of 3_{10} helicity than α helicity (≈ 1).^[15] The blueshifted π - π^* transition (208 to 205 nm) and a decrease in intensity of ellipticity at $\lambda=195$ nm, due to the perpendicular component of the exciton-split peptide π - π^* transition, are also typical of a 3_{10} helix. Because CD spectra were now concentration dependent (Figure 3 b), the ratio $\theta_{222}/\theta_{205}$ (inset) falling with in-

creasing concentration of **3**, this differently structured peptide bundle must be aggregating.

Nuclear magnetic resonance spectra can readily distinguish peptide backbone structures in solution, especially between α and 3_{10} helices.^[12,13] Although both conformations produce strong sequential NN($i,i+1$) and through space $\alpha\text{N}(i,i+3)$ NOEs, α and 3_{10} helices display different relative intensities for $\alpha\text{N}(i,i+4)$ and $\alpha\text{N}(i,i+2)$ correlations. ^1H NMR spectroscopic data for **3** (Figure 4 c) after 26 h, clearly estab-

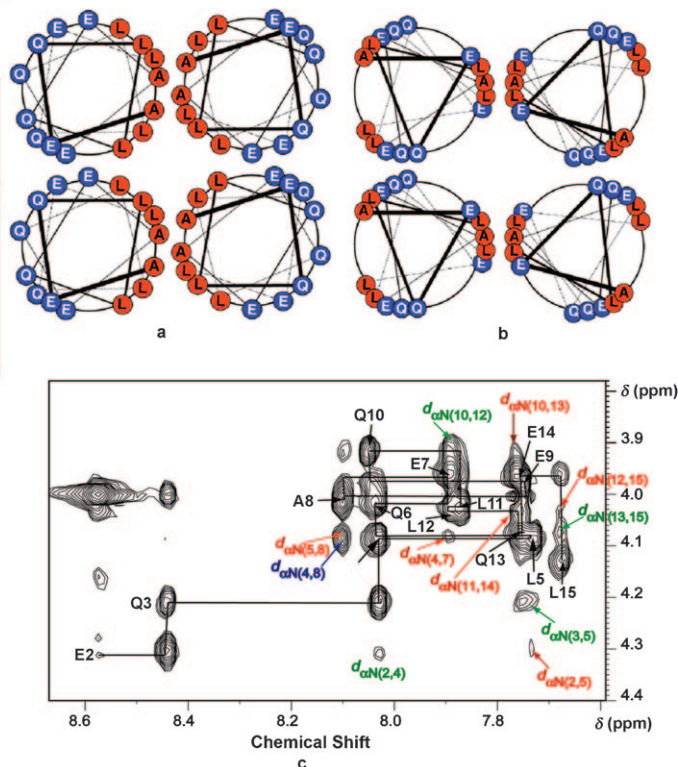


Figure 4. Helical wheels and partial 2D-NOESY spectrum of helix bundle **3**. Helical wheels for a 4-peptide bundle of α -helices (a) versus 3_{10} helices (b). The more elongated 3_{10} -helix bundle redistributes polar side chains of the amino acids to the interior of the 4-helix bundle and non-polar side chains to the exterior, leading to new intra-bundle hydrogen bonds between side chains and new inter-bundle hydrophobic packing of side chains. c) 2D-NOESY spectrum (αN region) for helix bundle **3** after 24 h at pH 4 showing formation of a 3_{10} helix. The spectrum corresponds to Figure 3 a (curve 4) for helix bundle **3** (50 mm phosphate buffer, 25% MeCN, pH 4) showing $\alpha\text{N}(i,i+2)$, green), $\alpha\text{N}(i,i+3)$, red), $\alpha\text{N}(i,i+4)$, blue) NOE correlations. The 3_{10} helicity is demonstrated by the preponderance of $\alpha\text{N}(i,i+2)$, green) and ($i,i+3$, red) NOEs and can be contrasted with Figure 3 c.

lish the presence of a 3_{10} -helical peptide, defined by pronounced $\alpha\text{N}(i,i+2)$ NOEs (Figure 4 c, green) specific for 3_{10} helicity, whereas $\alpha\text{N}(i,i+3)$, NN($i,i+2$) and $\alpha\beta(i,i+3)$ NOEs are consistent with a well-structured helix.^[12,13] Only a single, considerably weaker, $\alpha\text{N}(i,i+4)$ NOE (Figure 4 c, blue) typical for an α helix was present after 26 h. The pre-dominance of a 3_{10} -helix structure is confirmed by other NOEs between Gln-NH₂ and $\gamma\text{Me}(\text{Leu})$ and from Leu(side chain) to Glu/Gln(β,γ protons), because the side chains on

successive turns are exactly eclipsed in a 3_{10} helix due to an integral number of residues per turn. Amide coupling constants $^3J(\alpha\text{H},\alpha\text{NH})$ of 5–6 Hz, except for frayed N- and C-terminal residues ($^3J(\alpha\text{H},\alpha\text{NH})=6.3, 7.1$ Hz, respectively), support 3_{10} helices rather than α helices, which usually show smaller coupling constants.^[12a] A full three-dimensional structure determination was not possible due to spectral overlap and the high symmetry of the peptide sequence.

Together, the CD and NMR spectra clearly establish that a structural transformation from monomeric α helices to aggregated 3_{10} helices has occurred in the peptide backbones of **3** at 50–200 μM concentrations over 24 h at pH 4.

Conversion from 3_{10} helices to β sheets:

After 26 h, further changes occurred in the CD spectra. The molar ellipticity at $\lambda=222, 205, 195$ nm decreased with time, consistent with helix unwinding and the onset of formation of insoluble fibrils, until almost merging into the baseline after 5 d (Figure 3 a, curve 9). It has been reported that β strands tend to have almost featureless CD spectra due to antiparallel aligned carbonyl groups.^[16] Over the next 3 d (Figure 3 c), the solution was noticeably turbid and a concentration-dependent formation of fibrils in solution was visible by eye at this stage. Molar ellipticity ($\lambda_{\text{max}}=204, \lambda_{\text{min}}=223$ nm, Figure 3 a) were now of low intensity; subsequently, after 8 d θ_{200} began to decrease and the intensity of the minima at $\lambda=223$ nm increased rapidly over 14 d, indicative of another structural transition, probably the aggregation of β -sheet fibrils into thicker/wider fibers (Figure 3 d). A strong dominant $n\pi^*$ band was now visible at $\lambda \approx 223$ nm (Figure 3 d) typical of twisted β sheets. Fibrils filtered off and collected after 6 and 14 d were re-suspended in the same solvent and their thermal stability was examined by CD spectroscopy. At 25 $^{\circ}\text{C}$ both sets of fibrils gave CD spectra like typical β sheets (Figure 3 d). However, the fibrils collected after 6 d decomposed upon raising the temperature above 25 $^{\circ}\text{C}$, shown by loss of the CD signals (Figure 3 d), whereas this thermal instability was not present for fibrils aged for 14 d, their CD spectra being very similar over the temperature range 25–50 $^{\circ}\text{C}$ (Figure 3 d). This indicates that aged fibrils are thicker filaments with higher thermodynamic and structural stability.

The stability of the different products formed with time from **3** at pH 4 was briefly investigated by sonication, expected to disaggregate fibers by decreasing inter-peptide hydrogen bonding. Samples of **3** at the 4α -helical bundle stage

(within 10 h), sonicated for 15 s and examined by CD spectroscopy (Figure 5 a), showed no change in α helicity. Further sonication (2 \times 30 s) did not alter the CD spectra, sup-

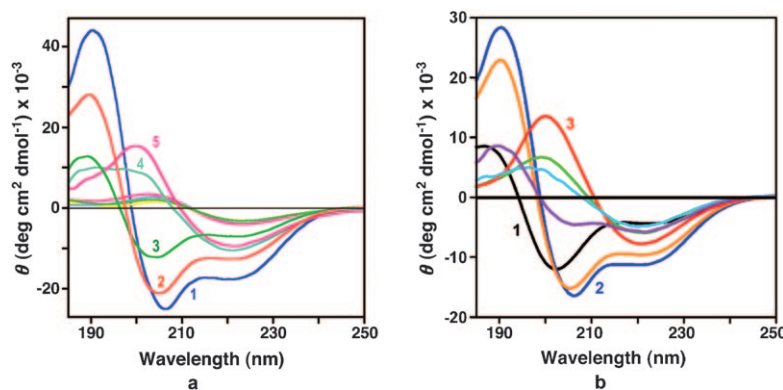


Figure 5. Effects of Sonication and pH on peptide bundle **3**. a) Far-UV CD spectra showing the effect of sonication on a solution of **3** (59 μM , in 50 mM phosphate buffer, 25% MeCN, 25 $^{\circ}\text{C}$, pH 4). Sonication of 3_{10} -helix-rich samples (curve 3) for 15 s gave CD spectra like curve 4 and further sonication produced β -turn-like curve 5. After 1 d, spectra were typical of β -sheet formation (close to baseline). b) Far-UV CD spectra of fibrils of **3** (50 mM phosphate buffer, 25% MeCN, 25 $^{\circ}\text{C}$) dissolved at pH 7 reverted to a spectrum (curve 1) typical of the 4α -helix bundle at pH 7. Re-acidification of this dissolved fibril solution to pH 4 gave predominantly a α -helical spectra (curve 2), which over time (1, 3.8, 6.8, 8.2 d) progressively gave changing spectra (orange, magenta, light blue, green, respectively) before giving a spectrum (curve 3) typical of β sheets. Further aging of the solutions produced spectra as shown in Figure 3 d (curves after 14 d).

porting the observations described above that the original 4α -helix bundle form of **3** is quite stable and not aggregated. Moreover, this sonication had no effect on the lag time that preceded the changes seen in Figure 3 a. However, when the 3_{10} helix form of **3** (aged for 2.5 d) was sonicated (15 s), the CD spectra changed to $\lambda_{\text{max}}=199$ nm and $\lambda_{\text{min}}=220$ nm, which both intensified upon sonication for an additional 30 s, the resulting CD spectrum being typical of a β turn (Figure 5 a, curve 5). This is not surprising because the tighter packing of the backbone in the 3_{10} helix than in an α helix forces the C=O \cdots H-N hydrogen bonds to point outward, away from the helical axis, resulting in decreased stability of the 3_{10} helix compared with the α helix.^[17] Because a 3_{10} helix is a combination of back-to-back β turns,^[18] some of these turns might be expected to be detectable during unwinding of a 3_{10} helix. After one day the molar ellipticity at $\lambda=199$ and 220 nm had decreased almost into the baseline consistent with β -strand formation and the CD spectrum typical of β sheets was subsequently obtained as the sample aged further in solution (Figure 5 a).

Interestingly, when fibrils were re-suspended in phosphate buffer at pH 7, they instantly became water-soluble with CD spectra that were quantitatively identical to fresh solutions of **3** at pH 7 (Figure 5 b, curve 1). Re-acidification of such solutions to pH 4 (Figure 5 b curve 2) gave CD spectral changes over time identical to those initially observed (Figure 3 a–d). Indeed, when solutions at any of the various stages described above were altered to pH 7, the CD spectra revert to identical spectra (Figure 5 b, curve 1) virtually instantaneously.

Fourier transform infrared (FTIR) analysis of structural changes: FTIR spectra were recorded over time and directly correlated with the CD spectra described above at the same time points. Figure 6 shows a time-course overlay of the im-

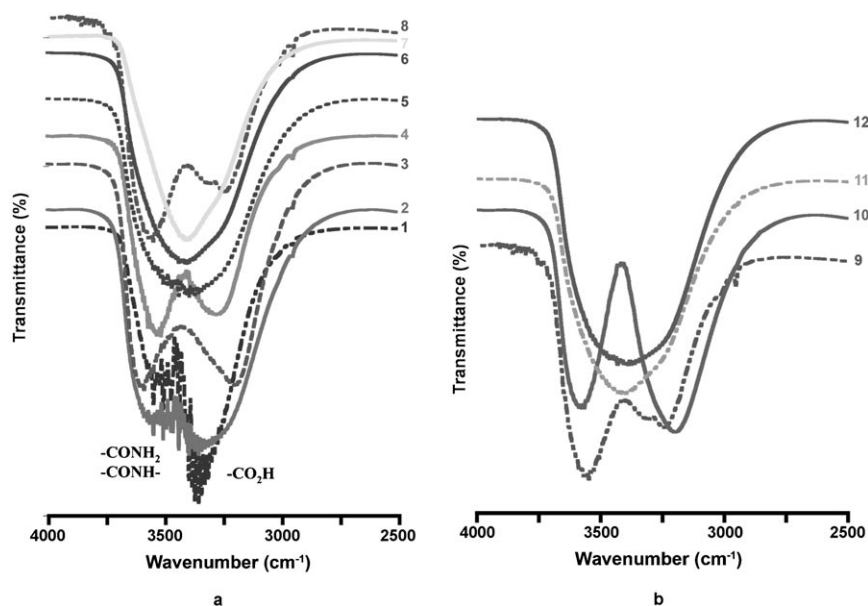


Figure 6. Time-dependent FTIR spectra (NH and OH region) for **3** in solution. a) Spectra at zero time (curve 1), 1 h (curve 2), 6 h (curve 3), then after 1 (curve 4), 2 (curve 5), 2.5 (curve 6), 4 (curve 7) and 5 d (curve 8; curve 9), corresponding to CD spectra shown in Figure 2a. b) Spectra after 5 (curve 9), 6 (curve 10), 7 (curve 11) and 8 d (curve 12) corresponding to CD spectra shown in Figure 3c. See the Supporting Information for this figure in colour.

portant amide NH and OH stretching frequencies, which are particularly important for understanding the hydrogen-bonding driving force behind α -helical to β -strand transformation. Spectral information for the important amide I and II bands are shown in the Supporting Information.

The initial solution of **3** at pH 4 ($t=0$ h) showed bands at $\tilde{\nu}=3502$ (amide NH stretch), 3350 (OH stretch) (Figure 6, curve 1) and 1654 cm^{-1} (amide I band, Figure S2 in the Supporting Information) typical of an α helix.^[19] Within 30 min, the carboxylic acid OH stretch vibration had broadened and shifted to lower wavenumber ($\tilde{\nu}=3300\text{ cm}^{-1}$) consistent with hydrogen bonding of the glutamic acid side chains within the helix bundle because it is un-aggregated at this stage according to concentration-independent CD spectra for 20–57 μM solutions (Figure S1 b in the Supporting Information). After 26 h, the FTIR spectra had significantly changed (Figure 6, curve 4) with absorptions at $\tilde{\nu}=3500\text{ cm}^{-1}$ (NH stretch), 3200 (OH stretch, indicative of hydrogen bonding Glu residues) and 1647 cm^{-1} (amide I band, Figure S2 in the Supporting Information), respectively, that are characteristic of a 3_{10} helix.^[20] These observations agree with the CD spectra and strongly support an α - to 3_{10} -helical transformation of the peptide backbone, driven by inter-helix hydrogen bonding of glutamic acid side chains. Because the CD spectra recorded after 26 h were concentration dependent, the 3_{10} -helix bundle must be in an aggregated form.

After this stage, as the solution aged, the NH band shifted to lower wavenumber and merged with the OH band, indicating involvement of both Glu and Glu side chains in hydrogen bonding (Figure 6, curve 5). At the β -strand stage (suggested by CD spectra) the NH and OH bands separated into two distinct bands. A narrower band at $\tilde{\nu}=3560\text{ cm}^{-1}$, indicative of non-hydrogen-bonded backbone NHs, and a more intense and slightly broader band at $\tilde{\nu}=3200\text{ cm}^{-1}$ (hydrogen bonding Glu residues and some hydrogen bonding Glu residues). This is not surprising because transition from α helix to β strand requires breaking of a considerable number of intramolecular backbone hydrogen bonds.

As the solution sample aged further, the NH and OH bands again merged, suggesting a further transformation. FTIR spectra of isolated fibrils had strong NH stretches ($\tilde{\nu}=3270$ – 3300 cm^{-1}) indicative of hydrogen-bonded amides, and amide I and II bands characteristic of parallel ($\tilde{\nu}=1637$ and 1556 cm^{-1} , respectively; Figure S3 in the Supporting Information) and intermolecular antiparallel ($\tilde{\nu}=1614$ – 1625 and 1537 cm^{-1} , respectively) β sheets,^[20,21] as observed for other aggregated proteins. A weak band at $\tilde{\nu}=1693\text{ cm}^{-1}$ signifies an antiparallel β -sheet structure,^[21] whereas the β -sheet amide I band $\tilde{\nu}=1614$ – 1625 cm^{-1} suggests strong hydrogen bonding. This supports intermolecular interactions between the 4-peptide bundles involving at least some antiparallel bundle alignments. Together with the CD spectra (Figures 3, 5), the FTIR spectra (Figure 6 and Figure S2 in the Supporting Information) strongly support formation of inter-bundle β -sheet aggregates as the sample ages at pH 4.

Transmission electron microscopy (TEM): Transmission electron micrographs were used to monitor the aging solutions of **3** at pH 4. Negatively stained aggregates showed formation of tiny fibrils in solutions of **3** at pH 4 within a few hours (Figure 7a), greatly increasing in number and thickness as the solution aged. The width ($\approx 5\text{ nm}$, Figure 7b) of these early fibers corresponds to the length of **3** if its four peptides are parallel β strands, indicating that the peptide backbone is perpendicular to, with β -sheet hydrogen bonding parallel to, the fiber axis. After days, these fibers were much longer (μm), twisted and surprisingly flexible (Figure 7c and d). Fibrils were unbranched, spiraling ribbons with left-handed twists repeating every 130 nm along their

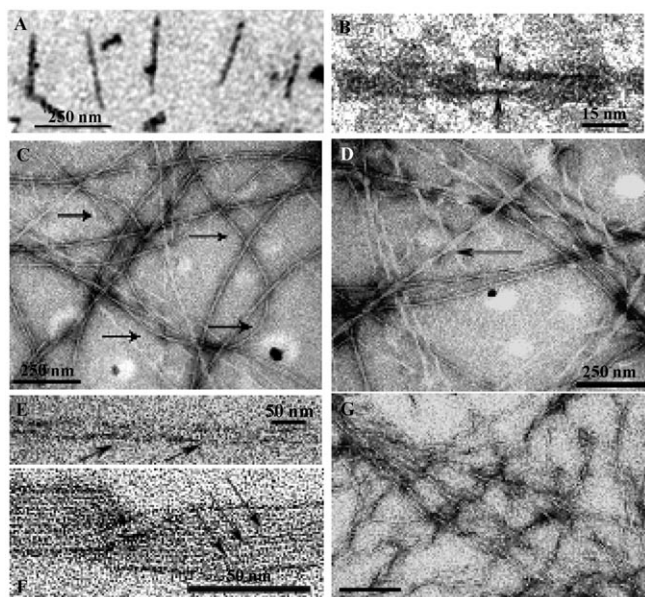


Figure 7. TEM of negatively stained (uranyl acetate) nanofibers of **3** (pH 4). A) Early forming fibers (≈ 30 – 250 nm long). B) One fiber ≈ 5 nm wide. C) More mature fibers curved (arrows) and μm long. D) Spiraling twisted ribbon fibers (arrow). E) Larger fiber with twists (arrows). F) 25 nm wide fiber showing finer ≈ 2.3 nm wide “strings” (arrows). G) Matted fibers after aging **3** at pH 4.0 for two weeks, scale bar = 250 nm.

axis (Figure 7e), as reported for amyloid fibrils.^[22] Higher magnification revealed multiple ≈ 2.3 nm thick filaments in fibrils, like strings in a rope (Figure 7f). Aged solutions produced matted fibers (Figure 7g) suggesting inter-ribbon interactions.

The fibrils that formed from **3** clearly exhibit classic TEM properties characteristic of amyloid structures. The 2.3 nm thickness corresponds to the cross-sectional dimension of **3** with parallel β strands, along the direction of side chain projection (Figure 8). First-order diffraction spots showed lattice spacing of 2.0 nm (Figure S4 in the Supporting Information), which established the relative arrangement of molecules within the fibrils, the cross β -sheet structure being typical of amyloid fibrils formed by naturally occurring proteins. Also typical of other amyloids, the fibrils bind to the chemical dye congo red^[23] but without yellow–green birefringence as also noted for amyloid fibrils from Sup35, the N terminus of Supp35 GNNQQNY, prions, peptides containing glutamine repeats^[24] and thioflavin T^[25] (not shown).

Conclusion

A key driving force in protein folding is the burying of hydrophobic residues in the interior of a protein, away from the solvating effects of water. In the case of an amphipathic peptide, aggregation is the simplest way of achieving this aim. In this study, four amphipathic peptides of identical sequence **1**^[3b] were assembled together in parallel alignment

to form peptide bundle **3** by using a macrocyclic template^[8] that is of appropriate size and shape to encourage intramolecular inter-peptide interactions.^[7c] This device has artificially promoted the aggregation of peptide **1** in that it is now part of a parallel aligned 4-peptide bundle **3**, a kinetically unfavourable process in the absence of the template, because there is no detectable aggregation of free peptide **1** alone at either pH 4 or 7. Assembling two such peptide chains in parallel on the cyclic template also leads to aggregation (data not shown), but much more slowly as would be expected if 4α -helix bundle formation is important for the process observed.

The ensuing conformational changes that occur at pH 4 for the 4-peptide “aggregate” **3** are not seen for the peptide **1** alone over at least twelve months at room temperature, but this may merely be an equilibrium problem reflecting low statistical probability of intermolecular peptide interactions in dilute solutions. Clearly, the peptide chains in the bundle communicate with one another through side chain to side chain interactions, which are responsible for the increased α helicity in the bundle versus the single peptide chain. In forming the 4-peptide bundle **3**, the amphipathic peptide can efficiently bury its hydrophobic Leu and Ala side chains within a stable 4α -helix bundle (Figure 4a), with hydrophilic Glu and Gln side chains oriented to the outside of the bundle for exposure to solvent. This 4α -helix bundle is monomeric at 20 – 57 μM concentrations (Figure S1 in the Supporting Information), whereas there is no evidence of concentration-dependent CD spectra that would be expected for an aggregating bundle.

However, the monomeric 4α -helix bundle **3** is not stable and undergoes a pH- and concentration-dependent transformation (Figures 3, 5) to nanofibers (Figure 7) composed of aggregated β sheets (Figures 3, 5, 7). This acid-dependent refolding to β sheets is reminiscent of neurodegenerative diseases where amyloidosis is often promoted by acidosis. The fibrils found herein display the same key features of other amyloids, including a cross β -sheet structure, unbranched, spiraling ribbons with repeating left-handed twists, age-related induction of thermally stable, matted fibers and the capacity to bind to dyes. Like some other amyloid-forming peptides, the peptide chains were organised in parallel alignment prior to the $\alpha \rightarrow \beta$ folding transition.

A very important finding was the detection in solution (by CD, NMR and FTIR spectroscopy) of 3_{10} helix, strand and sheet bundles as intermediates during the transformation of the 4α -helix bundle to the fibrillar aggregates. The preponderance of polar amino acids in the peptide aided solution solubility of these structural intermediates, which may otherwise have been water-insoluble. Correlative changes in the FTIR and CD spectra revealed that the 4α - to $4 \times 3_{10}$ -helix transformation at pH 4 was facilitated by hydrogen bonding of glutamic acid side chains, which began interacting within 30 min (Figure 6), whereas the helix bundle was monomeric. Furthermore, this transformation could be delayed by ≈ 4 d by addition of formic acid, a potential hydrogen-bonding competitor.

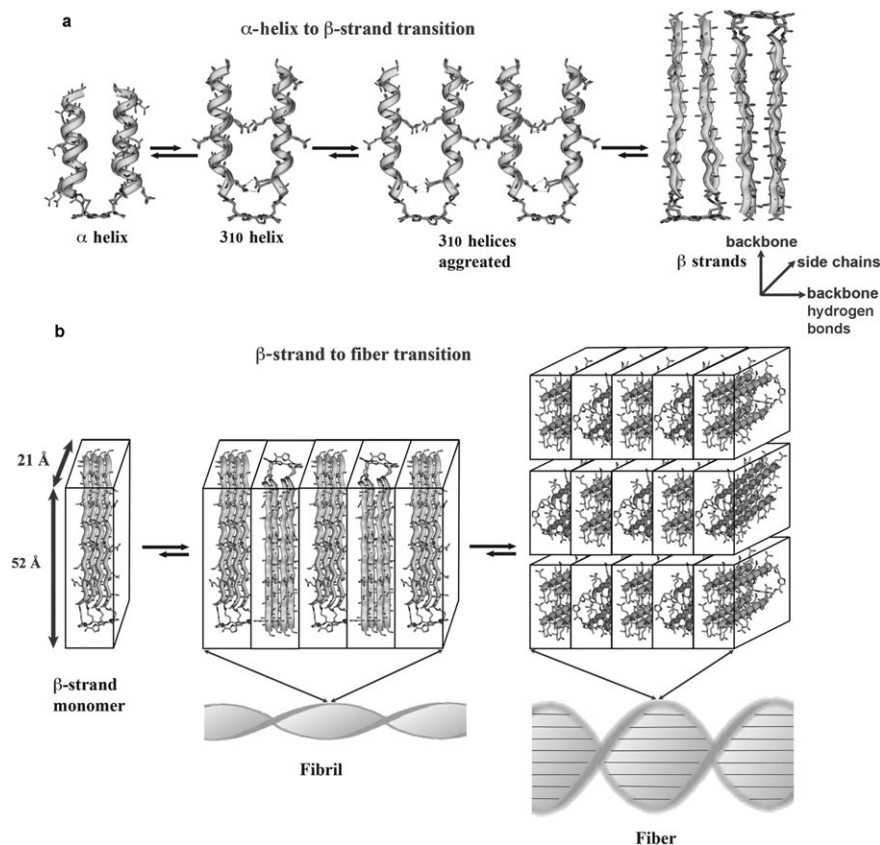


Figure 8. Model for conformational transitions of the 4-peptide bundle and assembly into amyloid fibrils. a) Equilibrium between α and 3_{10} helix is driven by aggregation-induced stabilisation of 3_{10} -helix bundles triggered by intra- and intermolecular hydrogen bonding of Glu then Gln side chains. Potentially solvent-exposed hydrophobic Leu and Ala side chains (not shown) that are redistributed to the outer exposed surfaces of the 3_{10} -helix bundle (Figure 4b) become buried through aggregation. Further elongation to β strands is driven by the greater thermodynamic stability of β -sheet aggregates that also involve hydrogen bonding by the peptide backbones aligned both parallel (shown intramolecular) and antiparallel (shown intermolecular). b) Model (not to scale) of how β -strand bundle **3** may form amyloid-like fibers with dimensions similar to those derived from TEM of fibrils (Figure 7); β -strands aggregate and form a fibril through peptide-backbone hydrogen bonding. Striated fibers then form from aggregation of fibrils through inter-fibril side chain interactions (hydrogen bonding and hydrophobic interaction). See the Supporting Information for this figure in colour.

We note that a bundle of four α helices distributes the peptide side chains in a distinctly different manner than four 3_{10} -helix bundles (Figure 4a vs. b), the latter redistribution enabling potential interactions between glutamic acid side chains on different chains but within the same 4-peptide bundle. Molecular models suggest that E2...E2 and E9...E9 hydrogen bonds are possible within a 3_{10} -helix bundle (Figure 8) that would then project L4, L5, A8 and L11 side chains to the outside solvent-exposed surface of the bundle, promoting aggregation of the 3_{10} -helical bundle **3**. We suggest that the 3_{10} -helix bundle, normally a thermodynamically unstable structure in comparison with the 4α -helix bundle, is stabilised by 1) intramolecular inter-chain hydrogen bonds between glutamic acid residues reorganised into close proximity and 2) intermolecular interactions between hydrophobic side chains that have as a consequence been redistributed to the solvent-exposed surfaces of the bundle.

Transformation of aggregated, stabilised 3_{10} -helix bundles to aggregated β strands occurs over the next 5 days as evidenced by CD and FTIR spectra. The 3_{10} helix is longer and narrower than an α helix, may be an intermediate in $\alpha \rightarrow \beta$ folding,^[26] but although easily accessed from an α helix, is not usually stable.^[12a,17,18] These longer bundled and aggregated 3_{10} helices are essentially back-to-back type III β turns.^[18] FTIR spectroscopy in particular indicates that as the 3_{10} -helix bundles aggregate and age, hydrogen-bonding patterns of the Glu and Gln residues change dynamically in line with peptide unfolding and refolding into longer extended β -strand intermediates towards β -sheet fibrils and fibers (Figure 8 and Figure S5 in the Supporting Information).

The results suggest that the elongated 3_{10} -helical regions of peptide backbones might be important unstable intermediates in the unwinding of the compressed secondary structure, the α helix, en route to the even more elongated β strand. This structural transition may play a fundamental role in facilitating refolding of α -helical regions of proteins and peptides through

transient, more elongated helices that need to aggregate for thermodynamic stability. Although formation of aggregated β sheets is thermodynamically more preferred, the entropic advantage provided by aggregation of α or 3_{10} helices might also be helpful in speeding up the folding transition(s). The rate of conversion of peptidic α helices to β sheets will be dependent upon a series of equilibria associated with α , aggregated α , aggregated 3_{10} and aggregated β structures. Clearly alignment of four equivalents of the Gln/Glu-rich amphipathic helical peptide discussed above was a key factor in being able to observe $\alpha \rightarrow \beta$ refolding and amyloid formation in this particular case. Bringing the peptides together on a template here, along with the capacity of α -helical Glu/Gln residues to form inter-peptide hydrogen bonds, were sufficient to form a stable peptide aggregate that was predisposed to conformational rearrangement. In other peptides, the hydrogen-bonding rearrangements that help bringing peptide chains together might be supplanted by hydrophobic interactions. It

remains to be seen if artificially encouraged alignments of other peptide sequences also convert to aggregated strands/sheets, but this seems very likely to us if the amino acid sequences also have strand/sheet propensity.

Experimental Section

General remarks: For general methods and materials see the Supporting Information.

Synthesis of compounds 1, 2 and 3: The 15-residue peptide **1** (AEQLL-QEAEQLLQEL-NH₂) was prepared by standard Fmoc (9-fluorenylmethoxycarbonyl) solid-phase peptide techniques by using Rink amide MBHA resin with 2-(1*H*-benzotriazole-1-yl)-1,1,3,3-tetramethyluronium hexafluorophosphate (HBTU) as a coupling reagent (see the Supporting Information for the free peptide RP-HPLC trace, Figure S6). Synthesis of **2** is given in the Supporting Information (Scheme S1, RP-HPLC trace shown in Figure S7). A novel feature of the synthesis of **3** was the reaction of resin-bound peptide **1** with cyclo-[Glu(OH)(Ox)]₄ (Ox = oxazole) in the presence of BOP and DIPEA. The helix bundle **3** was cleaved from the resin with a mixture of 95% TFA, 2.5% water and 2.5% triisopropylsilane, and purified by reversed phase HPLC (see the Supporting Information, RP-HPLC trace shown in Figure S8).

Characterisation data for compounds 1, 2 and 3

H-AEQLLQEAEQLLQEL-NH₂ (1): Peptide **1** was isolated off resin as a white solid (40 mg). ¹H NMR (600 MHz, CD₃CN/50 mM phosphate buffer (1:4), pH 4): δ = 8.50 (d, ³*J*(NH, α H) = 6.6 Hz, 1H; Glu- α NH), 8.42 (d, ³*J*(NH, α H) = 6.2 Hz, 1H; Gln- α NH), 8.07 (d, ³*J*(NH, α H) = 4.4 Hz, 1H; Ala- α NH), 8.04 (m, 2H; Leu- α NH, Glu- α NH), 7.99 (d, ³*J*(NH, α H) = 5.3 Hz), 1H; Glu- α NH), 7.91 (d, ³*J*(NH, α H) = 5.2 Hz, 1H; Gln- α NH), 7.85 (d, ³*J*(NH, α H) = 5.6 Hz, 1H; Gln- α NH), 7.81 (d, ³*J*(NH, α H) = 6.0 Hz, 1H; Leu-NH), 7.83 (d, ³*J*(NH, α H) = 4.0 Hz, 1H; Leu-NH), 7.83 (d, ³*J*(NH, α H) = 4.8 Hz, 1H; Leu-NH), 7.79 (m, 2H; Gln- α NH, Glu- α NH), 7.74 (d, ³*J*(NH, α H) = 7.0 Hz, 1H; Leu- α NH), 4.31 (m, 1H; Glu- α H), 4.21 (m, 1H; Gln- α H), 4.14 (m, 1H; Leu- α H), 4.12 (m, 1H; Leu- α H), 4.10 (m, 1H; Leu- α H), 4.09 (m, 1H; Gln- α H), 4.06 (m, 1H; Glu- α H), 4.04 (m, 1H; Leu- α H), 4.03 (m, 1H; Ala- α H), 4.02 (m, 1H; Gln- α H), 4.02 (m, 1H; Leu- α H), 4.01 (m, 1H; Glu- α H), 3.99 (m, 1H; Leu- α H), 3.98 (m, 1H; Gln- α H), 3.95 (m, 1H; Glu- α H), 2.26–2.57 (m, overlap, 16H; Gln- γ H, Glu- γ H), 1.99–2.12 (m, overlap, 14H; Gln- β H, Glu- β H), 1.93 (m, 2H; Gln- β H, Glu- β H), 1.69 (m, 5H; Leu- β H), 1.59 (m, 5H; Leu- β H), 1.51 (m, 5H; Leu- γ H), 1.44 (d, ³*J*(α H, β H) = 7.0 Hz, 3H; Ala- β H), 1.39 (d, ³*J*(α H, β H) = 7.2 Hz, 3H; Ala- β H), 0.78–0.87 ppm (m, overlap, 30H; Leu- γ CH₃); MS (ISMS): *m/z* (%): 585.3 [*M*+3*H*]³⁺/3, 877.4 [*M*+2*H*]²⁺/2, 1753.9 [*M*+*H*]⁺; HRMS: *m/z*: calcd for C₇₆H₁₂₉N₂₀O₂₇⁺ [*M*+*H*]⁺ 1753.9331; found: 1753.9346; HPLC (3.33%/min linear gradient starting from 0% B (0.1% TFA in 10% water/acetonitrile): *R*₁ = 23.7 min (Vydac 218TP54 C18 column), *R*₂ = 23.7 min (Phenomenex Luna 5 μ C18 column) (see the Supporting Information, Figure 6).

Cyclo-[Glu(OH)(Ox)]₄ (2): Compound **2** was isolated as a white solid (1.0 g, 86%). ¹H NMR (600 MHz, [D₆]DMSO): δ = 8.00 (s, 4H; Ox-H), 7.79 (d, ³*J*(NH, α CH) = 8.3 Hz, 4H; Glu- α NH), 4.67 (m, 4H; Glu- α H), 1.74 (m, 8H; Glu- γ H), 1.64 ppm (m, 8H; Glu- β H); ¹³C NMR (150.9 MHz, [D₆]DMSO): δ = 173.77 (Glu- γ CO₂H), 163.90 (Ox C-2), 159.85 (CO-N), 142.54 (Ox CH-5), 135.46 (Ox C-4), 45.89 (Glu- α CH), 30.05 (Glu- γ CH₂), 27.54 ppm (Glu- β CH₂); MS (ISMS): *m/z* (%): 785.2 [*M*+*H*]⁺; HRMS: calcd for C₃₂H₃₃N₈O₁₆⁺ [*M*+*H*]⁺: 785.2009; found: 785.1986; HPLC (3.33%/min linear gradient starting from 0% B): *R*₁ = 15.4 min (Vydac 218TP54 C18 column), *R*₂ = 17.2 min (Phenomenex Luna 5 μ C18 column) (see the Supporting Information, Figure 7).

4-Helix Bundle 3: Compound **3** was isolated as a white solid (140 mg, 71%). ¹H NMR (600 MHz, CD₃CN/50 mM phosphate buffer (1:4), pH 4) (chemical shifts are ordered by α NH, α H, β H, γ H, δ H) δ = 8.44 (d, ³*J*(NH, α H) = 5.8 Hz, 1H; Gln- α NH), 8.03 (d, ³*J*(NH, α H) = 4.2 Hz, 1H; Leu- α NH), 7.87 (d, ³*J*(NH, α H) = 4.8 Hz, 1H; Leu- α NH), 8.04 (d,

³*J*(NH, α H) = 4.1 Hz, 1H; Gln- α NH), 7.89 (d, ³*J*(NH, α H) = 4.7 Hz, 1H; Glu- α NH), 8.10 (d, ³*J*(NH, α H) = 4.2 Hz, 1H; Ala- α NH), 7.76 (d, ³*J*(NH, α H) = 5.0 Hz, 1H; Glu- α NH), 8.05 (d, ³*J*(NH, α H) = 4.6 Hz, 1H; Gln- α NH), 7.87 (d,

³*J*(NH, α H) = 4.4 Hz, 1H; Leu- α NH), 7.89 (d, ³*J*(NH, α H) = 4.7 Hz, 1H; Leu- α NH), 8.03 (d, ³*J*(NH, α H) = 4.1 Hz, 1H; Gln- α NH), 7.75 (d, ³*J*(NH, α H) = 4.5 Hz, 1H; Glu- α NH), 7.68 (d, ³*J*(NH, α H) = 7.1 Hz, 1H; Leu- α NH), 4.30 (m, 1H; Glu- α H), 4.21 (m, 1H; Gln- α H), 4.08 (m, 1H; Leu- α H), 4.04 (m, 1H; Leu- α H), 4.01 (m, 1H; Gln- α H), 3.96 (m, 1H; Glu- α H), 4.01 (m, 1H; Ala- α H), 3.97 (m, 1H; Glu- α H), 3.92 (m, 1H; Gln- α H), 4.04 (m, 1H; Leu- α H), 4.03 (m, 1H; Leu- α H), 4.04 (m, 1H; Gln- α H), 4.00 (m, 1H; Glu- α H), 7.68 (m, 1H; Leu- α H), 1.93 (m, 2H; Glu- β H), 1.95, 2.08 (m, 2H; Gln- β H), 1.65 (m, 2H; Leu- β H), 2.37 (m, 2H; Gln- β H), 2.11, 2.04 (m, 2H; Glu- β H), 1.43 (d, ³*J*(β H, α H) = 7.3 Hz, 3H; Ala- β H), 2.13, 2.08 (m, 2H; Glu- β H), 2.12, 2.04 (m, 2H; Gln- β H), 1.73 (m, 2H; Leu- β H), 1.77 (m, 2H; Leu- β H), 2.14, 2.10 (m, 2H; Gln- β H), 1.74 (m, 2H; Glu- β H), 2.35 (m, 2H; Glu- γ H), 2.32 (m, 2H; Gln- γ H), 1.53 (m, 1H; Leu- γ H), 1.72 (m, 1H; Leu- γ H), 2.12, 2.06 (m, 2H; Gln- γ H), 2.39, 2.30 (m, 2H; Glu- γ H), 2.43, 2.33 (m, 2H; Glu- γ H), 2.49, 2.38 (m, 2H; Gln- γ H), 1.66 (m, 1H; Leu- γ H), 1.54 (m, 1H; Leu- γ H), 2.42, 2.33 (m, 2H; Gln- γ H), 2.55 (m, 2H; Glu- γ H), 1.74 (m, 1H; Leu- γ H), 0.90, 0.85 (d,

³*J*(γ H δ H) = 5.8 Hz, 6H; Leu- δ H), 0.83, 0.86 (d, ³*J*(γ H δ H) = 5.8 Hz, 6H; Leu- δ H), 0.87, 0.84 (d, ³*J*(γ H δ H) = 6.5 Hz, 6H; Leu- δ H), 0.83 (d, ³*J*(γ H δ H) = 6.1 Hz, 6H; Leu- δ H), 0.84 ppm (d, ³*J*(γ H δ H) = 6.8 Hz, 6H; Leu- δ H); MS (ISMS): *m/z* (%): 2575.7 [*M*+3*H*]³⁺/3; HRMS: calcd for C₃₃₆H₅₃₉N₈₈O₁₂₀₃⁺ [*M*+3*H*]³⁺/3: 2575.6181, found: 2575.6223; HPLC (3.33%/min linear gradient starting from 0% B): *R*₁ = 24.2 min (Vydac 218TP54 C18 column), *R*₂ = 24.3 min (Phenomenex Luna 5 μ C18 column) (see the Supporting Information, Figure 8).

Circular dichroism spectroscopy: CD measurements were performed by using a Jasco model J-710 spectropolarimeter, which was routinely calibrated with (1*S*)-(+)-10-camphorsulfonic acid. The peptide **1** and compound **3** were dissolved in 50 mM phosphate buffer/25% MeCN (peptide concentrations 2–100 μ M) at pH 4 and 7.1. Spectra were recorded at room temperature (298 K), with a 0.1 cm Jasco quartz cell over the wavelength range 260–185 nm at 50 nm min⁻¹ with a bandwidth of 1.0 nm, response time of 1 s, resolution step width of 0.1 nm and sensitivity of 20–50 mdeg. Each spectrum represents the average of five scans with smoothing to reduce noise.

Nuclear magnetic resonance spectroscopy: NMR spectra for the peptide AEQLLQEAEQLLQEL-NH₂ and compound **3** were recorded on a Bruker Avance 600 spectrometer in 25% CD₃CN/50 mM phosphate buffer at 298 K. Proton assignments were made by using TOCSY (80 ms mixing time) and NOESY (300, 420 ms mixing time). Watergate solvent suppression was used and all spectra were processed by using Xwinnmr.

Fourier transform infrared spectrometry (FTIR): FTIR spectra were recorded at room temperature on a Jasco Fourier Transform IR 460 plus spectrometer with a 2 cm⁻¹ resolution, in the wavelength range of 4000–1000 cm⁻¹. The solutions (25 μ L) were placed between CaF₂ plates as a thin film and the data were collected. Typically, 64 scans were averaged for a single spectrum.

Electron microscopy: Assembled filaments precipitated at pH 4.0 formed defined β -sheet nanofibers in solution. Aliquots of sample were applied to a glow discharged carbon coated 200 mesh grid and blotted for negative staining with 1% uranyl acetate in water. A Tecnai 12 transmission electron microscope (FEI, Netherlands) operating at 100 keV recorded micrograph images at 98000 and 30000 magnifications on Kodak SO 163 electron image film or directly to CCD (Soft Imaging system megaview camera). Selected micrograph areas were further digitised on a Nikon 8000 digital scanner (Nikon Inc.) at 4000 dpi. The image processing IMAGIC software package (Image Science, Germany) was used to display Fourier transforms of selected regions that show first-order diffraction spots with a lattice spacing of 2.0 nm, indicating the fibril is more ordered in one direction, (see the Supporting Information, Figure S4).

Acknowledgements

We thank the Australian Research Council (ARC) and the Australian National Health and Medical Research Council (NHMRC) for partial funding of this work and the ARC for a Federation Fellowship to D.P.F.

- [1] a) R. S. Harrison, P. C. Sharpe, Y. Singh, D. P. Fairlie, *Rev. Physiol. Biochem. Pharmacol.* **2007**, *159*, 1–77; b) F. Chiti and C. M. Dobson, *Annu. Rev. Biochem.* **2006**, *75*, 333–366; c) F. Chiti, C. M. Dobson, *Nat. Chem. Biol.* **2009**, *5*, 15–22; d) P. T. Lansbury, H. A. Lashuel, *Nature* **2006**, *443*, 774–779; e) D. Otzen, P. H. Nielsen, *Cell. Mol. Life Sci.* **2008**, *65*, 910–927; f) D. M. Fowler, A. V. Koulov, W. E. Balch, J. W. Kelly, *Trends Biochem. Sci.* **2007**, *32*, 217–224; g) I. W. Hamley, *Angew. Chem.* **2007**, *119*, 8274–8295; *Angew. Chem. Int. Ed.* **2007**, *46*, 8128–8147.
- [2] D. M. Fowler, A. V. Koulov, C. Alory-Jost, M. S. Marks, W. E. Balch, J. W. Kelly, *PLoS Biol.* **2006**, *4*, e6.
- [3] a) M. R. Sawaya, S. Sambashivan, R. Nelson, M. I. Ivanova, S. A. Siemers, M. I. Apostol, M. J. Thompson, M. Balbirnie, J. J. Wiltzius, H. T. McFarlane, A. O. Madsen, C. Riek, D. Eisenberg, *Nature* **2007**, *447*, 453–457; b) U. Baxa, R. B. Wickner, A. C. Steven, D. E. Anderson, L. N. Marekov, W. M. Yau, R. Tycko, *Biochemistry* **2007**, *46*, 13149–13162; c) D. J. Gordon, J. J. Balbach, R. Tycko, S. C. Meredith, *Biophys. J.* **2004**, *86*, 428–434; d) C. Wasmer, A. Lange, H. Van Melckebeke, A. B. Siemer, R. Riek, B. H. Meier, *Science* **2008**, *319*, 1523–1526; e) J. Madine, A. Copland, L. C. Serpell, D. A. Middleton, *Biochemistry* **2009**, *48*, 3089–3099; f) K. Iwata, T. Fujiwara, Y. Matsuki, H. Akutsu, S. Takahashi, H. Naiki, Y. Goto, *Proc. Natl. Acad. Sci. USA* **2006**, *103*, 18119–18124; g) B. Vestergaard, M. Groenning, M. Roessle, J. S. Kastrup, M. van de Weert, J. M. Flink, S. Frokjaer, M. Gajhede, D. I. Svergun, *PLoS Biol.* **2007**, *5*, e134; h) T. Sasaki, E. T. Kaiser, *J. Am. Chem. Soc.* **1989**, *111*, 380–381; i) M. Lieberman, T. Sasaki, *J. Am. Chem. Soc.* **1991**, *113*, 1470–1471.
- [4] a) J. Johansson, *Swiss Med. Wkly.* **2003**, *133*, 275–282; b) J. W. Kelly, *Curr. Opin. Struct. Biol.* **1996**, *6*, 11–17; c) J.-C. Rochet, P. T. Lansbury, Jr., *Curr. Opin. Struct. Biol.* **2000**, *10*, 60–68; d) Y. Fezoui, D. M. Hartley, D. M. Walsh, D. J. Selkoe, J. J. Osterhout, D. B. Teplow, *Nat. Struct. Mol. Biol.* **2000**, *7*, 1095–1099; e) T. Takeda, D. K. Klimov, *Proteins Struct. Funct. Bioinf.* **2009**, *77*, 1–13; f) A. Andreola, V. Bellotti, S. Giorgetti, P. Mangione, L. Obici, M. Stopponi, J. Torres, E. Monzani, G. Merlini, M. Sunde, *J. Biol. Chem.* **2003**, *278*, 2444–2451; g) B. Ciani, E. G. Hutchinson, R. B. Sessions, D. N. Woolfson, *J. Biol. Chem.* **2002**, *277*, 10150–10155; h) Y. Fezoui, D. B. Teplow, *J. Biol. Chem.* **2002**, *277*, 36948–36954; i) Q.-x. Hua, M. A. Weiss, *J. Biol. Chem.* **2004**, *279*, 21449–21460; j) K. Pagel, S. C. Wagner, K. Samedov, H. von Berlepsch, C. Bottcher, B. Kokschi, *J. Am. Chem. Soc.* **2006**, *128*, 2196–2197; k) D. C. Tahmassebi, T. Sasaki, *J. Org. Chem.* **1998**, *63*, 728–731.
- [5] a) S. Jones, J. Manning, N. M. Kad, S. E. Radford, *J. Mol. Biol.* **2003**, *325*, 249–257; b) W. Hoyer, T. Antony, D. Cherny, G. Heim, T. M. Jovin, V. Subramaniam, *J. Mol. Biol.* **2002**, *322*, 383–393; c) B. Gerhartz, I. Ekiel, M. Abrahamson, *Biochemistry* **1998**, *37*, 17309–17317; d) M. Yazaki, J. Varga, P. J. Dyck, M. D. Benson, *Amyloid* **2002**, *9*, 268–271.
- [6] C. C. Huang, P. W. Faber, F. Persichetti, V. Mittal, J. P. Vonsattel, M. E. MacDonald, J. F. Gusella, *Somatic Cell Mol. Genet.* **1998**, *24*, 217–233.
- [7] a) G. Tuchscherer, M. Mutter, *J. Pept. Sci.* **2005**, *11*, 278–282; b) E. S. Seo, J. C. Sherman, *Biopolymers* **2007**, *88*, 774–779; c) A. K. Wong, M. P. Jacobsen, D. J. Winzor, D. P. Fairlie, *J. Am. Chem. Soc.* **1998**, *120*, 3836–3841.
- [8] Y. Singh, N. Sokolenko, M. J. Kelso, L. R. Gahan, G. Abbenante, D. P. Fairlie, *J. Am. Chem. Soc.* **2001**, *123*, 333–334.
- [9] a) M. Mutter, A. Chandravarkar, C. Boyat, J. Lopez, S. Dos Santos, B. Mandal, R. Mimna, K. Murat, L. Patiny, L. Saucedo, G. Tuchscherer, *Angew. Chem.* **2004**, *116*, 4267–4273; *Angew. Chem. Int. Ed.* **2004**, *43*, 4172–4178; b) M. S. Camus, S. Dos Santos, A. Chandravarkar, B. Mandal, A. W. Schmid, G. Tuchscherer, M. Mutter, H. A. Lashuel, *ChemBioChem* **2008**, *9*, 2104–2112.
- [10] a) C. Gribbon, K. J. Channon, W. Zhang, E. F. Banwell, E. H. Bromley, J. B. Chaudhuri, R. O. Oreffo, D. N. Woolfson, *Biochemistry* **2008**, *47*, 10365–10371; b) R. A. Kammerer, D. Kostrewa, J. Zurdo, A. Detken, C. Garcia-Echeverria, J. D. Green, S. A. Muller, B. H. Meier, F. K. Winkler, C. M. Dobson, M. O. Steinmetz, *Proc. Natl. Acad. Sci. USA* **2004**, *101*, 4435–4440.
- [11] C. A. Rohl, R. L. Baldwin, *Methods Enzymol.* **1998**, *295*, 1–26.
- [12] a) G. L. Millhauser, C. J. Stenland, P. Hanson, K. A. Bolin, F. J. van de Ven, *J. Mol. Biol.* **1997**, *267*, 963–974; b) H. Kessler, S. Seip in *Two-Dimensional NMR Spectroscopy: Applications for Chemists and Biochemists*, 2nd ed. (Eds.: W. R. Croasmun, R. M. K. Carlson), Wiley, **1994**, pp. 619–654.
- [13] K. Wüthrich, *NMR of Proteins and Nucleic Acids*, Wiley, New York, **1986**.
- [14] G. Tuchscherer, L. Scheibler, P. Dumy, M. Mutter, *Biopolymers* **1998**, *47*, 63–73.
- [15] C. Toniolo, A. Polese, F. Formaggio, M. Crisma, J. Kamphuis, *J. Am. Chem. Soc.* **1996**, *118*, 2744–2745.
- [16] N. Sreerama, S. Y. Venyaminov, R. W. Woody, *Protein Sci.* **1999**, *8*, 370–380.
- [17] Z. Biron, S. Khare, A. O. Samson, Y. Hayek, F. Naider, J. Anglister, *Biochemistry* **2002**, *41*, 12687–12696.
- [18] A. Moretto, F. Formaggio, B. Kaptein, Q. B. Broxterman, L. Wu, T. A. Keiderling, C. Toniolo, *Biopolymers* **2008**, *90*, 567–574.
- [19] P. Juszczak, A. S. Kolodziejczyk, Z. Grzonka, *J. Pept. Sci.* **2009**, *15*, 23–29.
- [20] E. M. Castano, C. Soto, B. Frangione, N. C. Inestrosa, *J. Biol. Chem.* **1995**, *270*, 3063–3067.
- [21] N. Yamada, K. Ariga, M. Naito, K. Matsubara, E. Koyama, *J. Am. Chem. Soc.* **1998**, *120*, 12192–12199.
- [22] C. Blake, L. Serpell, *Structure* **1996**, *4*, 989–998.
- [23] W. E. Klunk, J. W. Pettegrew, D. J. Abraham, *J. Histochem. Cytochem.* **1989**, *37*, 1273–1281.
- [24] a) M. Balbirnie, R. Grothe, D. S. Eisenberg, *Proc. Natl. Acad. Sci. USA* **2001**, *98*, 2375–2380; b) S. Chen, V. Berthelie, J. B. Hamilton, B. O’Nuallain, R. Wetzel, *Biochemistry* **2002**, *41*, 7391–7399.
- [25] H. LeVine, III, *Methods Enzymol.* **1999**, *309*, 274–284.
- [26] O. Tcherkasskaya, W. Sanders, V. Chynwat, E. A. Davidson, C. S. Orser, *J. Biomol. Struct. Dyn.* **2003**, *21*, 353–366.

Received: August 30, 2010

Published online: December 15, 2010